A 10 kW Inductive Wireless Power Transfer Prototype for EV Charging in Thailand

Jutturit Thongpron[1†], **Wuttikai Tammawan**[2], **Teerasak Somsak**[3], **Wiwat Tippachon**[2], **Kosol Oranpiroj**[1], **Ekkachai Chaidee**[4], and **Anon Namin**[2], Non-members

ABSTRACT

The electric vehicle (EV) market is rising despite the COVID-19 pandemic in Thailand and the rest of the world. The Energy Policy and Planning Office, Ministry of Energy, is supporting the development of EV charging stations in Thailand. However, recent research published by Thais on the subject does not involve more than 1.24 kW wireless power transfer (WPT), whereas commercial EVs need at least 3.5 kW charging facilities. This study aims to develop a 10 kW WPT for EV charging in Thailand. The experimental procedure firstly required the design of block ferrite EE55 cores. Secondly, the transmitter and receiver coils were constructed from homemade Litz wire. Thirdly, the prototype magnetic parameters were measured and simulated. A 10 kW high-frequency inverter was then built and tested. The 10 kW prototype IPT system was subsequently simulated, constructed, and characterized. The results revealed that when the prototype IPT system was applied to the resistive tungsten halogen load during the first stage of the research, at 369.4 V DC input voltage and 32.33 A DC input current, the DC output voltage, and currents were 362.4 V and 29.67 A, respectively, while the maximum DC output power and the dc-to-dc efficiency equated to 10.75 kW and 90.00%, respectively.

Keywords: Wireless Power Transfer, Wireless EV Charger, Inductive Wireless Power Transfer

1. INTRODUCTION

In 2020, the EV global market rose, thereby increasing EV registrations by 41% despite the COVID-19 pandemic and this figure is expected to reach 10 million EVs worldwide by the end of the decade. There are three reasons for the creation of a supportive regulatory framework for the zero-emission vehicle (ZEV): the additional incentive of an economic turndown, the expansion of EV models, falling battery cost. The important point is that the EV needs access to charging stations, but the charger type and location are not specific to the user's EV. There are residence, enterprise, and public charging points. The household and company slow charging points were 9.5 million and represented 40 GW at homes and more than 15 GW at workplaces by approximately. Under the sustainable development scenario, there are plans to install 20 million slow chargers and 4 million fast public chargers by 2030 [1].

Wireless power transfer (WPT) technology that does not require the physical connection between transmitter and receiver is advantageous for wireless EV charging [2]. WPT EV charging is safe to operate, saves the environment, and convenient for use with automated charging [3]. In addition, WPT EV charging may be safe for touchable objects or surfaces of charging equipment that may contain droplets from COVID-19 infected users.

Following Nikola Tesla's WPT invention, more than 14,000 papers have been published on "wireless power transfer" [4], with over 75% of these in the last five years [5]. There are many wireless power transfer applications in portable electric apparatus such as the solar tricycle, bus, car, vessel, TV, and smartphone [6, 7].

A review of the publications on the stationary wireless charging EV system reveals that PATH developed a 60 kW WPT with 60% efficiency (η). While the KAIST-OLEV reached 180 kW WPT with $\eta = 80\%$ for stations and roads, and the Utah State University and SELECT tested the 30 kW WPT for buses. In addition, UNPLUGGED developed a 50 kW station. The world champions in wireless EV charging stations range from 30 to 180 kW WPT [8–10].

The publications on IPT systems use rated power of 1 kW [2], 5 kW, 7.7 kW, 11 kW, 22 kW, 50 kW, and 100 kW from national laboratories, research centers, and universities at the frequency range of 20 to 150 kHz, air gap of 100 to 265 mm in the circular coupler DD, solenoid, square, bipolar, and rectangular cores and coils. The dc-to-dc and grid-to-battery efficiency reported in these

Manuscript received on September 1, 2021; revised on October 2, 2021; accepted on October 6, 2021. This paper was recommended by Associate Editor Yuttana Kumsuwan.

[1]The authors are with the Clean Energy System Research Unit (CES-RMUTL) and Division of Electrical Engineering, Rajamangala University of Technology Lanna Chiang Mai, 50300 Chiang Mai, Thailand.

[2]The authors are with the Clean Energy System Research Unit (CES-RMUTL) and Division of Electrical Engineering, Rajamangala University of Technology Lanna Chiang Rai, 57120 Chiang Rai, Thailand.

[3]The author is with the Clean Energy System Research Unit (CES-RMUTL) and College of Integrated Science and Technology, Rajamangala University of Technology Lanna Chiang Mai, 50300 Chiang Mai, Thailand.

[4]The author is with the Department of Electrical Engineering, King Mongkut's University of Technology Thonburi, 10140 Bangkok, Thailand.

[†]Corresponding author: jutturit@rmutl.ac.th

Digital Object Identifier: 10.37936/ecti-eec.2022201.246108

publications ranged from 80 to 96.5%, with the coil-to-coil efficiency of 93 to 98% [9, 10].

Commercial companies have produced high power IPT prototypes during the last decade [11], such as WiTricity 3.7 kW, 2013 [12], Toshiba 7 kW, 2014 [13], BOSCH 7 kW, 2015 [14], WiTricity 11 kW, 2016 [15], Fraunhofer ISE 22 kW, 2015 [16], ONRL 50 and 120 kW, 2018 [17, 18], Bombardier 200 kW, 2016 [19], and Wave 250 kW, 2019 [20].

Whereas light-duty EV charging needs chargers with a rated power of 3.5 kW, 7.2 kW, 10 kW, 22 kW, or higher, the wireless EV charging station requires a minimum power of 3.5 kW WPT for operation.

The magnetic cores that increase permeability and reduce leakage flux for the IPT are made from air core [5–7], ferrite core [2, 3], magnetic nanoparticle core [21], flexible magnetic core [22], and magnetic concrete core [23]. The IPT core shapes reported in existing publications were made from the ferrite bases of plate, bar, and tile but the concept of blocked construction in commercial magnetic ferrite application has never previously been reported. This work proposes the scaling up of the blocked U-shape from the commercial EE55 ferrite cores.

The 2021 IPT developments for EV charging have involved not only the design of high power wireless transfer but also dynamic charging [24], optimized magnetic core [25], triple coils [26], and compensation parameters tuning [27, 28]. Power electronics have been applied to IPT EV charging systems such as a novel three-phase rectifier design for IPT [29], a novel output regulation for three phases three-level IPT [30], voltage control primarily by IPT [31], implementation of fundamental harmonic approximation for IPT [32], DC-DC topology interfacing for IPT [33], a high-frequency zero-voltage switching technique for IPT with variable phase shift control [34], and real-time implementation of an IPT on-demand shuttle service [35]. Thermal analysis and a safety study have also been reported for wireless power transfer development [36, 37], and so on.

The various articles published worldwide in 2021 on wireless EV charging tend to focus on the core and coil design, application of power electronics, thermal analysis, and safety studies. However, there is a lack of studies on wireless EV charging station development in Thailand.

The EV is gaining attention in Thailand due to its energy savings capability, environment-friendliness, high technology, and low service cost [38]. Moreover, the battery cost and charging infrastructure are the main points for customers deciding to buy an EV [39]. There are 4,800 BEV and 172,200 HPEV registers in Thailand, and only cable plug-in chargers have been installed in 647 public charging stations, including 1,974 charging outlets as of the end of 2020 [40].

The Energy Policy and Planning Office (EPPO), Ministry of Energy, Thailand, is promoting and supporting the EV market by installing EV charging stations, preparing legal regulations and rules, as well as developing EV batteries and wireless EV charging stations.

The first wireless power transfer charger in Thailand was developed in 2014 for the 14 W e-scooter [41]. Subsequently, WPT chargers developed by Thais include the 1,240 W wireless EV [2], the 12 W WPT [5], the 10 W for solar tricycles [6], 30 W for TV [7], 230 W for motorcycles [42], the 324 W for e-bikes [43], the 82 W distance-frequency WPT [44], the 110 W phase shift WPT [45], the 289 W multi-transmitter WPT [46], the 1,000 W primary and secondary controlled WPT [47], the automated efficiency 540 W [48], and the 200 W kitchen appliance [49]. However, static WPT of more than 1,240 W is required for EV charging stations.

The Wireless Electric Vehicle Battery Charging Station project, supported by the EPPO, has been implemented to conduct experiments on EV charging and improve Thailand's competitiveness. The challenge at this stage is to scale up our previous 1,240 W [2] to 10,000 W WPT for wireless EV charging.

This study proposes the block UU shape using the commercial EE55 ferrite core for high power IPT coils. This technique can shorten the ferrite core sintering and casting process which has to be made to order, resulting in high cost. The prototype uses the ferrite parts of commercial electronics since these are faster than the made-to-order ferrite core. Moreover, the ferrite core of the IPT coils can produce a higher flux linkage between Tx and Rx, or a higher magnetic coupling coefficient than the air core IPT. The ferrite core IPT system can be operated when installed on the chassis of the EV. While the air core IPT may change the performance of the IPT system, the flux linkage changes direction through the iron and steel structure when installed on the EV. In addition, this study can improve the capability of IPT development, through core and coil design and analysis, power electronics application, and IPT system evaluation. Furthermore, impacts of the proposed WPT for EV charging stations in Thailand may include building decision-making confidence in customers looking for ZEVs. This study should act as an inspiration to other researchers to start to seriously consider the construction of high power IPT prototype.

This paper presents the development of a 10 kW WPT for EV charging in Thailand. Firstly, we propose inductive wireless power transfer (IPT) as the building blocks of IPT system integration, core design and construction, coil design, and output power and efficiency analysis. Secondly, we report on the experiments involving magnetic coefficients and mutual inductance, inverter efficiency, and IPT system integration. Finally, we present a comparison of the experimental results between the IPT prototype's DC output power and dc-to-dc efficiency.

2. INDUCTIVE WIRELESS POWER TRANSFER

WPT technology can be divided into four types: (a) inductive wireless power transfer (IPT), (b) capacitive

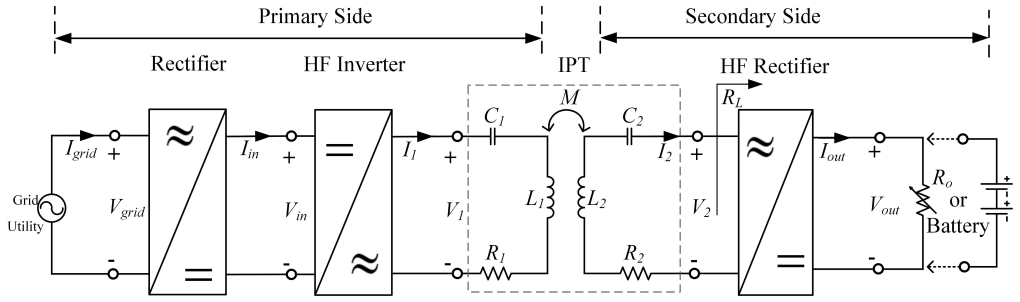

Fig. 1: *Building blocks of the IPT system.*

wireless power transfer (CPT), (c) light wireless power transfer (such as visible, infrared, or laser lights), and (d) microwave wireless power transfer [50]. This study focuses on the IPT that transfers energy through a magnetic field. The IPT operates as a high-frequency transformer with a high air gap range.

This section presents the building blocks and efficiency of the IPT, its design and construction, high-frequency inverter, and the output power and efficiency of the system.

2.1 Building Blocks and Efficiency of the IPT System

The simple building blocks of the IPT system connecting to the grid utility consist of a rectifier, a high-frequency (HF) inverter, IPT coils, and the load or battery of the EV, as shown in Fig. 1.

The efficiency of the EV WPT system is defined by the off-board input and power supply of the control electronics. The AC grid utility or DC power supply bus connects to the terminals of the electrical load, such as with a battery or device on the EV or secondary side, according to IEC 61980-1 standards [50]. Two efficiency definitions: "grid-to-battery efficiency (η_{G2B})" and "dc-to-dc efficiency ($\eta_{dc-to-dc}$)" [8], can be derived by:

$$\eta_{G2B} = \frac{P_{out}}{P_{grid}} \tag{1}$$

$$\eta_{dc-to-dc} = \frac{P_{out}}{P_{in}} \tag{2}$$

In this study, the output power of the prototype is defined by the $\eta_{dc-to-dc}$ calculated from the DC input power and the DC output of the IPT system.

2.2 Design and Construction of the IPT Core

The goal of the prototype IPT system for EV charging in Thailand is to transfer 10 kW of electrical energy through an air gap of at least 150 mm, which is the distance between the charging station and the chassis of the EV. The IPT technology is applied in this study due to our previous experience with electrical machines.

Firstly, we focus on what happens when our 1.5 kW EE55 transformer operates in the event an air gap exists between the EE cores. The 5 mm air gap, representing half of the pole shoe distance between the middle and left or right leg, produces the best performance. Secondly, the IPT core is built to transfer magnetic energy through the 150 mm air gap, where the distance between the pole shoes of the core leg should be more than twice the 150 mm or 300 mm. We used eight of the EE cores in the order arrangement to obtain a distance of 432 mm between the two legs of the U-shaped core model. This concept was proposed in [2], to transfer energy of 1.24 kW at 160 mm.

In this study, we focus on building greater power transfer of 1.24 kW (the manufacturer's specifications rate is 1.75 kW) using the first IPT core model. The single row of eight EE55 cores produces the same average values of magnetic field intensity (H) and magnetic flux density (B) along with all EE55 cores. The EE55 core rows are increased from one row to six to transfer more flux through the air gap.

To answer the question: Which is the best, between the EE55 and the bar or cube ferrite core? The bar or cube ferrite core has better density because it can be built into the solid block model, but the EE55 has windows that act as air gaps in the IPT core. However, the EE55 has been produced by many manufacturers. A reliable MnZn soft ferrite product is chosen for this study where the saturation flux density B is 510 mT at H of 1,194 A/m. The manufacturer produces the EE 55 core in the largest size, while the ferrite bar or cube is made to order. The quantity of ferrite core used in this work is lower than the minimum bar or cube of the made-to-order product. However, the difference in cost between the ferrite bar or cube and the EE55 core is not significant since the same materials and transportation costs are involved, but the mass or volume varies [51].

Nevertheless, the design core sintering construction is the preferred process, aligning with the best practice of the "Shaped Magnetic Field in Resonance, SMFIR" technology proposed by the KAIST, Korea [52].

The IPT design in this study is constructed of a block UU-shaped EE55 ferrite core. Fig. 2(a) shows the single EE55 core with a 0.5 cm air gap. The block UU shape of 12 EE55 put in series with a 160 mm air gap [2] is illustrated

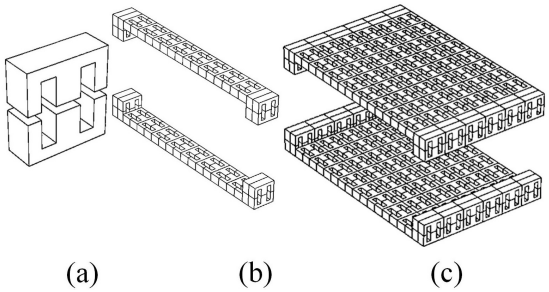

Fig. 2: *Construction of the IPT cores; (a) the single EE55 core with a 0.5 cm air gap, (b) the block UU shape of 12 EE55 put in series with a 160 mm air gap [2], and (c) scaling up to a 10 kW level IPT core.*

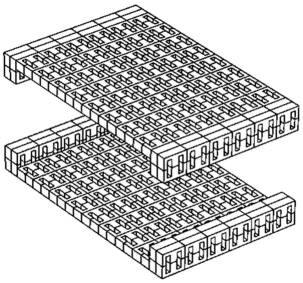

Fig. 3: *The 10 kW IPT core model.*

in Fig. 2(b) and scaling up to a 10 kW level IPT core in Fig. 2(c). The six parallel rows of the block UU shape with a 160 mm air gap is used for the prototype core in this study. Fig. 3 shows the prototype 10 kW IPT core model.

2.3 Design of IPT Coils

The coils of the IPT can be divided into two categories: primary and secondary, wound in the same turns to become the symmetry parameters. The homemade Litz wire is constructed of 41 SWG 18 enamel copper wires and cotton insulation tape for both the primary and secondary coils, wound in 18 turns, as shown in Fig. 4.

Fig. 5 demonstrates the assembly of the primary and secondary cores and coils.

2.4 Magnetic Field and Flux Simulation

The magnetic field and flux are simulated in this study using the three dimensions of finite element software from COMSOL Multiphysics. The parameters of mutual inductance (M), magnetic coupling coefficient (k), field intensity (H), and flux density (B) are evaluated using the simulation results. Fig. 6 shows the simulation results of the magnetic field and flux.

The simulation results provided by the software can be evaluated as (a) the flux linkage between the primary and secondary coils and the values of the coupling coefficient (k) and mutual inductance (M) of the IPT. These values need to be applied in calculating the performance of the IPT coils presented in Section 2.5. (b) The contour lines and color shades of the magnetic flux density (B) and magnetic field intensity (H) can be evaluated using the

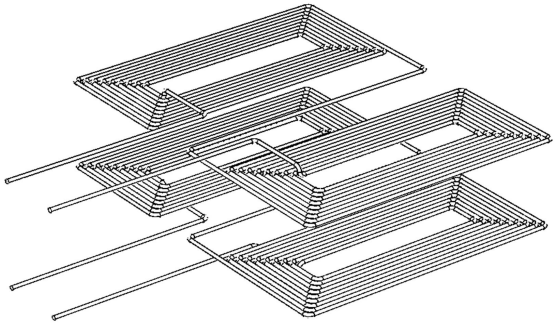

Fig. 4: *The 10 kW IPT coil design.*

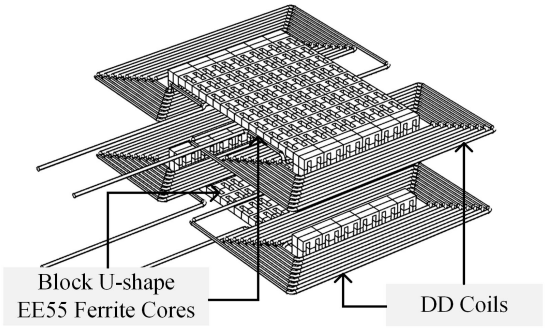

Fig. 5: *Assembly of the IPT cores and coils.*

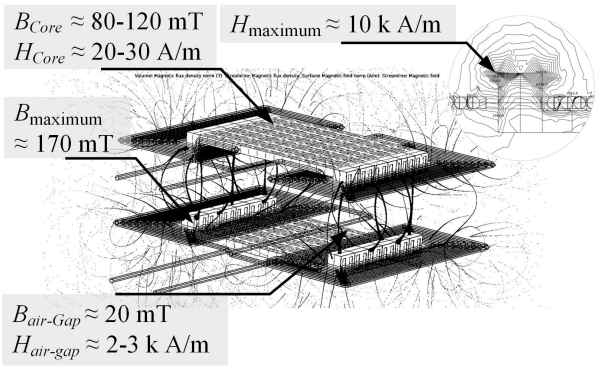

Fig. 6: *Simulation results for magnetic field intensity and flux density.*

COMSOL software. The maximum values of B and H in the inner and outer surface of the magnetic core or in the air gap can be compared with the values in the datasheet or specifications.

In this study, the average B ranges from 80 to 120 mT in the ferrite core and 20 mT in the air gap. While the average H ranges from 20 to 30 A/m in the core and 2 to 3 kA/m in the air gap. The specifications B and H of the EE55 core are 510 mT and 1,192 A/m, respectively. However, the maximum B was 170 mT at the inner angle of the pole legs of the Tx and Rx cores, while the maximum H reached 10 kA at the skin of the pole shoe edges, as shown in Fig. 6.

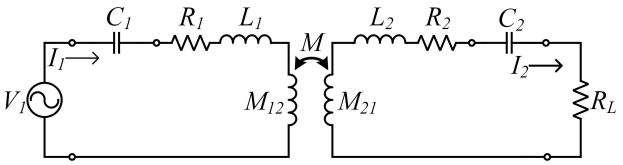

Fig. 7: *Equivalent circuit of the IPT coils.*

2.5 Characteristics of the IPT Coils

The positions of the primary and secondary coils are defined by distance z, the misalignment in the forward direction of x, and misalignment in the transverse to the left of y, according to the IEC 61980-1 standards [50]. The magnetic linkage between the primary and secondary coils is parametric according to the coupling coefficient (k). The mutual inductance (M) of the primary and secondary coils can be defined as

$$M(x,y,z) = k(x,y,z)\sqrt{L_1 L_2}. \tag{3}$$

The equivalent circuit of the IPT is presented in Fig. 7. The transmitter (Tx), as the primary component of the IPT, consists of the primary resonant capacitor (C_1), primary parasitic resistance (R_1), primary leakage reactance (L_1), and primary mutual inductance (M_{12}). Similarly, the receiver (Rx) consists of the secondary resonant capacitor (C_2), secondary parasitic resistance (R_2), secondary leakage reactance (L_2), and secondary mutual inductance (M_{21}). The mutual inductance (M) of the primary and secondary coils is equal to the M_{12} and M_{21}, as shown in Eq. (4) and Fig. 7.

$$M(x,y,z) = M_{12}(x,y,z) = M_{21}(x,y,z). \tag{4}$$

When the IPT is supplied by the input voltage (V_1) and the angular frequency (ω) source, it must operate in the resonant conditions using the C_1, and C_2, calculated as

$$\begin{aligned} C_1 &= \frac{1}{\omega^2 \cdot L_1} \\ C_2 &= \frac{1}{\omega^2 \cdot L_2}. \end{aligned} \tag{5}$$

From Fig. 7, the primary and secondary impedances, currents, and voltages of the IPT can be determined by

$$\begin{bmatrix} Z_1 & -j\omega M(x,y,z) \\ -j\omega M(x,y,z) & Z_2 \end{bmatrix} \begin{bmatrix} I_1 \\ I_2 \end{bmatrix} = \begin{bmatrix} V_1 \\ 0 \end{bmatrix} \tag{6}$$

where Z_1 and Z_2 are defined as

$$Z_1 = \left[R_1 + j\left(\omega L_1 - \frac{1}{\omega C_1} \right) \right] \tag{7}$$

$$Z_2 = R_2 + R_L + j\left(\omega L_2 - \frac{1}{\omega C_2} \right) \tag{8}$$

The I_1 and I_2 are derived from Eq. (6), as

$$I_1 = \frac{V_1 Z_2}{Z_1 Z_2 + (\omega M(x,y,z))^2} \tag{9}$$

$$I_2 = \frac{j\omega M(x,y,z) V_1}{Z_1 Z_2 + (\omega M(x,y,z))^2} \tag{10}$$

The input power of the IPT is shown in Eq. (11) while the output power is shown in Eq. (12), and IPT efficiency calculated by Eq. (13).

$$P_{1-coil} = \frac{\left[R_1 (R_2 + R_L)^2 + (\omega M(x,y,z))^2 (R_2 + R_L) + {X_2}^2 R_1 \right] V_1^2}{\left[R_1 (R_2 + R_L) - X_2 X_1 + (\omega M(x,y,z))^2 \right]^2 + \left[X_2 R_1 + X_1 (R_2 + R_L) \right]^2} \tag{11}$$

$$P_{2-coil} = \frac{(\omega M(x,y,z))^2 V_1^2 \cdot R_L}{\left[R_1 (R_2 + R_L) - X_2 X_1 + (\omega M(x,y,z))^2 \right]^2 + \left[X_2 R_1 + X_1 (R_2 + R_L) \right]^2} \tag{12}$$

$$\eta_{IPT} = \eta_{C2C} = \frac{(\omega M(x,y,z))^2 \cdot R_L}{\left[R_1 \left[(R_2 + R_L)^2 + {X_2}^2 \right] + (\omega M(x,y,z))^2 (R_2 + R_L) \right]} \tag{13}$$

Eqs. (3) to (13) are derived to describe the circuit parameters of the IPT coils. From the IPT construction, the magnetic coupling with high-frequency resonant conditions, output power, and coil efficiency can be evaluated by Eqs. (12) and (13).

Eq. (12) is used to analyze the output power of the IPT coils as the output resistive load function as well as the square of the frequency, mutual impedance, HF input voltage, and proportions of the IPT circuit impedance parameters.

Eq. (13) describes the effect of the output resistive load, square of the frequency and mutual impedance, and IPT circuit impedance parameters. The maximum conditions of the IPT coils, coil-to-coil efficiency or their values may be derived from the derivatives of this equation according to these IPT circuit parameters.

Moreover, Eqs. (12) and (13) derived from Eqs. (3) to (11) are validated using the MATLAB Simulink.

2.6 High-Frequency (HF) Square Wave Inverter

The H-bridge square wave inverter, scaled up from previous work [5], is used for the 10 kW IPT. The square wave inverter injects the sinusoidal current waveform into the IPT [5] through the resonance conditions controlled by C_1 and C_2, as shown in Eq. (5). The performance of the high-frequency pulse inverter can be evaluated using the MATLAB Simulink, as shown in Fig. 8.

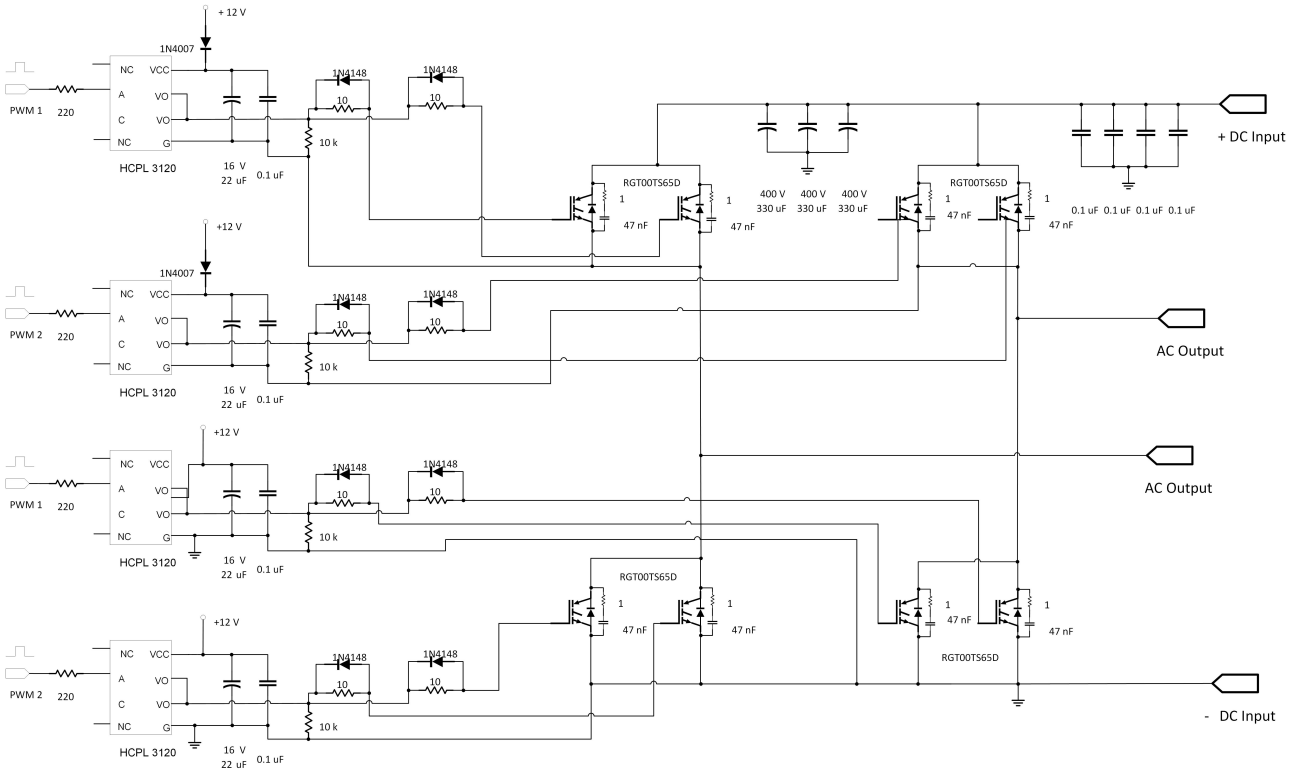

Fig. 8: *The 10 kW, 20 kHz pulse inverter design.*

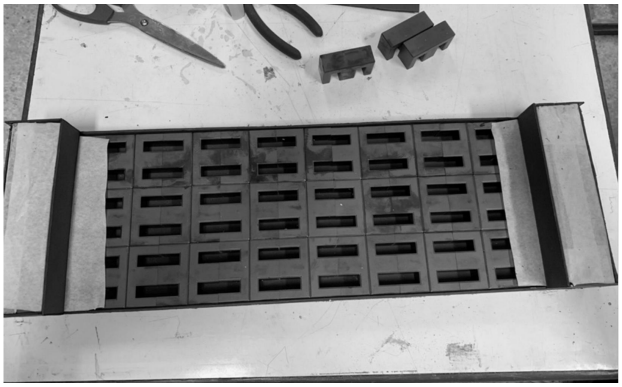

Fig. 9: *The 10 kW block EE55 core assembly.*

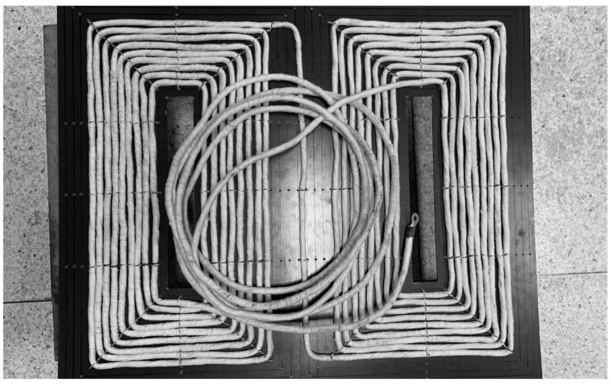

Fig. 10: *The 10 kW homemade Litz wire assembly.*

3. EXPERIMENT

In the experiment, the model cores of the prototype 10 kW level IPT were first constructed. Secondly, the design coils were assembled. Thirdly, the magnetics parameters of the prototype 10 kW IPT were measured, and the 10 kW, 20 kHz pulse inverter then constructed and tested. Finally, the prototype 10 kW IPT was characterized to determine the power-input voltage and output efficiency.

3.1 Construction of the 10 kW Block UU Cores

The high-frequency EE55 ferrite cores were assembled into the block to perform the UU shape for the IPT primary and secondary cores. The frames of the U-shaped block were made from a 3 mm vulcanized fiber insulator, as shown in Fig. 9.

3.2 Construction of the 10 kW Spiral Coils

The Litz wire was constructed from 41 conductors of SWG 18 copper wires, twisted and bounded using cotton tape. The Litz wires were rectangular, turning on the Bakelite and tightened by cable ties, as shown in Fig. 10.

3.3 Measurement of Magnetic Parameters

When the Tx and Rx of the 10 kW level IPT were positioned at 0, 0, and 160 mm as shown in Fig. 11, the $M(0, 0, 160)$ of the two coils was measured using a KEYSIGH E4980L Precision LCR Meter. The series adding

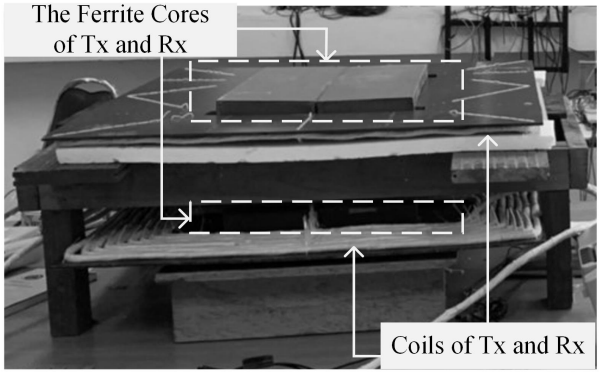

Fig. 11: *The 10 kW primary and secondary IPT Coils at 0, 0, and 160 mm.*

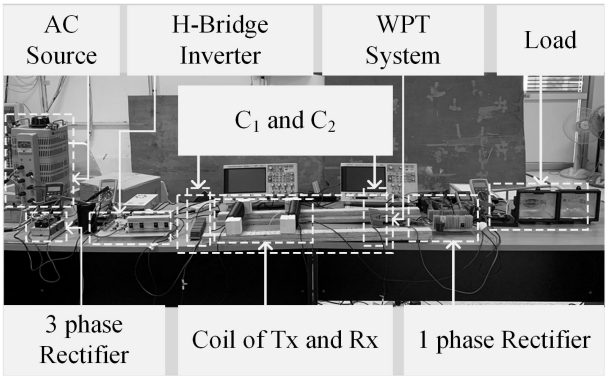

Fig. 12: *Power electronics kit setup.*

and series opposing technique was used to determine the $M(x, y, z)$ values ranging from 20 to 300 mm or 0, 0, and 20 mm to 0, 0, and 300 mm positions. The k of the IPT was calculated by Eq. (3). Fig. 12 presents the experimental power electronics kit setup.

3.4 Construction and Testing of the 10 kW HF Square Wave Inverter

The 10 kW, 20 kHz pulse inverter has been scaled up from the previous work [2]. The power switches were parallel to the two IGBT RGT00TS65DGC11 to supply a higher current at the switching frequency of 20 kHz. The HCPL3120 optocouplers drove the gate pulse signals with 1 μs dead time using the TMS320F28379D microcontroller. Fig. 13 shows the system integrations of the square wave inverter.

The square wave inverter was tested for resistive load and output-input voltage characterization. The output power and efficiency of the inverter were then evaluated.

3.5 Characterization of the Prototype 10 kW IPT

Firstly, the prototype 10 kW IPT system was evaluated using the MATLAB Simulink. Secondly, the IPT system was integrated with a varied input voltage power supply, three-phase rectifier, HF square wave inverter, IPT primary and secondary coils, secondary HF rectifier, and the resistive load. The building block is shown in Fig. 1.

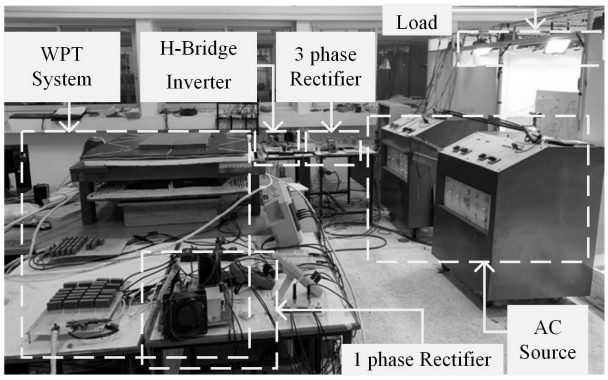

Fig. 13: *IPT coils and resistive load setup.*

Table 1: *Parameters of the prototype IPT system.*

Parameter	Definition	Value	Unit
R_1	Internal resistance of L_1	0.242	Ω
R_2	Internal resistance of L_2	0.23	Ω
L_1	Inductor transmitting loops	202.9	μH
L_2	Inductor receiving loops	206.4	μH
C_1	Capacitor transmitting loops	312.1	nF
C_2	Capacitor receiving loops	306.81	nF
N	Number of coil turns	18	turns
z	Distance between Tx and Rx	160	mm
M	Mutual inductance of the IPT system	75.475	μH
k	Coupling coefficient	0.37	
f	Switching frequency	20	kHz
R_O	Load resistance	2.66–12.21	Ω
V_{in}	Inverter DC input voltage	20–369	V

The prototype 10 kW IPT for EV charging in Thailand was evaluated using the tungsten halogen lamp resistive load to test the performance of the output power-input voltage and system efficiency-output power characteristics for the first stage. The next step of evaluating the battery charging performance will be tested in future work. The prototype 10 kW IPT experimental setup is shown in Fig. 13.

Table 1 shows the circuit parameters of the prototype IPS system in this study.

4. RESULTS AND DISCUSSION

The results of the 10 kW IPT prototype for EV charging in Thailand include the $M(x, y, z)$ and $k(x, y, z)$ measurements, HF inverter output power and efficiency, DC output power-DC input voltage, and dc-to-dc efficiency characteristics.

4.1 Mutual Inductance and Coupling Coefficient

The $M(x, y, z)$ and the $k(x, y, z)$ of the IPT for measuring the positions along 0, 0, and 20 mm to 0, 0, and 300 mm in steps of 20 mm are shown in Fig. 14. The $M(0, 0, 20)$ was 220 μH, decreasing along the position to $M(0, 0, 60)$ due to the linkage and leakage of the flux between Tx to Rx drastically changing the direction.

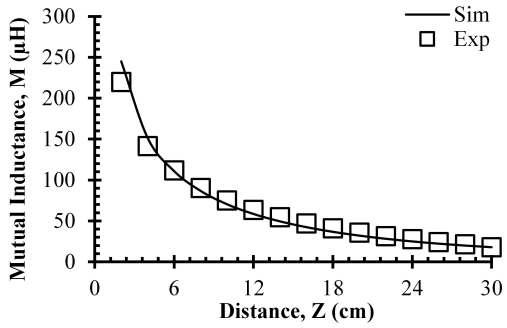

Fig. 14: *Simulation and experimental results for the mutual inductance-distance characteristics of the IPT.*

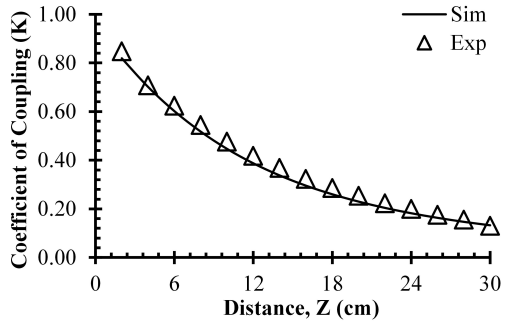

Fig. 15: *Simulation and experimental results of the coupling coefficient-distance characteristics for the IPT.*

The $M(0,0,8)$ to $M(0,0,300)$ decreased slightly. The $M(x,y,z)$ versus z characteristics are shown in Fig. 14.

The k of the IPT is shown in Fig. 15, with the $k(0,0,20)$ being about 0.84 and then declining when the z was increasing due to the exponential change in the flux link.

The simulation results obtained by the COMSOL software for $M(x,y,z)$ and the $k(x,y,z)$ were similar to those from the experiment. Eqs. (3) and (4) accord with the physical positioning of Tx and Rx, as shown in Figs. 14 and 15.

4.2 Output and Efficiency of the HF Inverter

The output waveforms of the HF inverter tested for the tungsten halogen lamp resistive load are shown in Fig. 16.

The squared wave with an amplitude of 243 V at 20 kHz was the output voltage waveform (ch1) of the HF inverter. The output current waveform (ch2) of the HF inverter shows the *R-C* integrator characteristic effect of the tungsten halogen resistive load. The drop in voltage on the inverter IGBT switches (ch3) demonstrates the amplitude of 272 V with a bit of spike voltage.

Fig. 17 shows the output power of the HF inverter reaching 10 kW at an input voltage of 250 V. The output power rose when the input voltage increased exponentially because the output power is in direct variation to the square of voltage ($P = V^2/R$).

Fig. 18 shows the efficiency-output power characteristics of the HF inverter. The inverter's efficiency rose to 90%, along with the 2 kW to 10 kW output power.

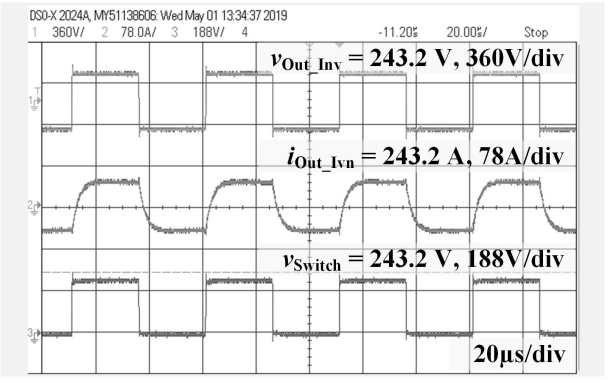

Fig. 16: *Testing waveforms of the pulse inverter.*

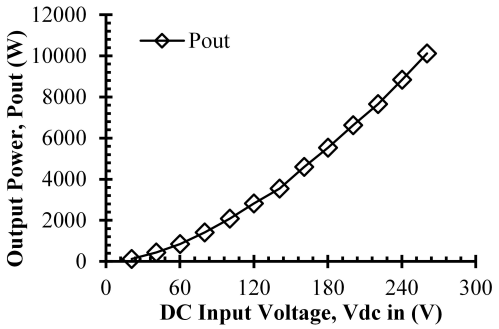

Fig. 17: *Testing output power-input voltage characteristics of the pulse inverter.*

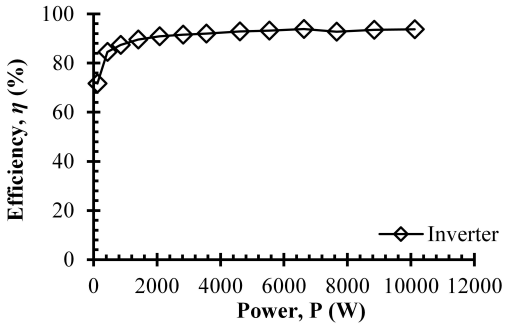

Fig. 18: *Testing efficiency-output power characteristics of the pulse inverter.*

The simulation and experimental results are similar for the output power-input voltage (Fig. 17) and efficiency-output power (Fig. 18) characteristics of the pulse inverter.

4.3 Performance of the Prototype 10 kW IPT

The waveforms of the prototype 10 kW IPT coil input and output current and voltage are shown in Fig. 19. The input voltage (ch1) is represented by the square wave with an amplitude of 376 V 20 kHz. However, the input current waveform (ch2) of 35.6 A was sinusoidal because the IPT operated in resonance conditions. On the other hand, the output voltage waveform (ch3) represented the square wave of 386 V since the current source character-

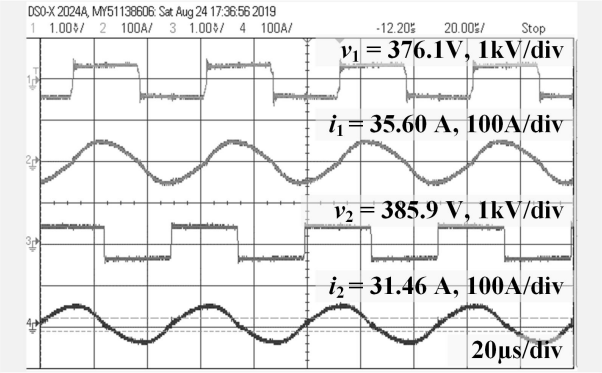

Fig. 19: *Testing waveforms of the 10 kW IPT.*

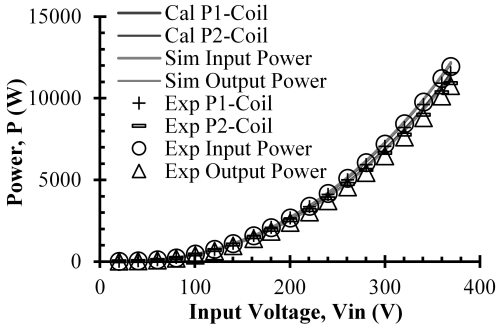

Fig. 20: *Current-grid input voltage characteristics of the IPT system.*

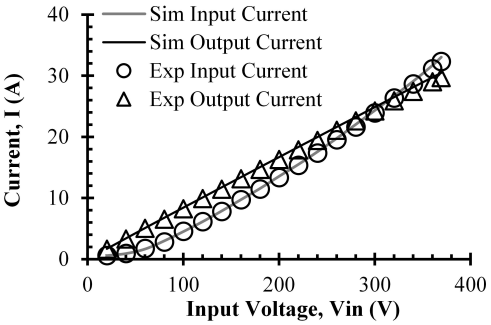

Fig. 21: *DC output power-input voltage characteristics of the IPT system, and the maximum output power of 10.75 kW.*

istics of the IPT injected the resonant sinusoidal current into the HF rectifier circuit. Furthermore, the output current waveform of 31.5 A was a resonant sinusoidal wave.

The characteristics of the output power and input voltage of the IPT are shown in Fig. 20. The MATLAB Simulink simulation results differed slightly from the experiment. The input increased the output power exponentially due to the relationship of $P = V^2/R$ shown in Eq. (12). At an input voltage of 369.4 V, the DC output power of the prototype IPT system was 10.75 kW.

The input and output currents of the prototype 10 kW coils are the function of the input voltage, in accordance with Eqs. (9) and (10), as shown in Fig. 21.

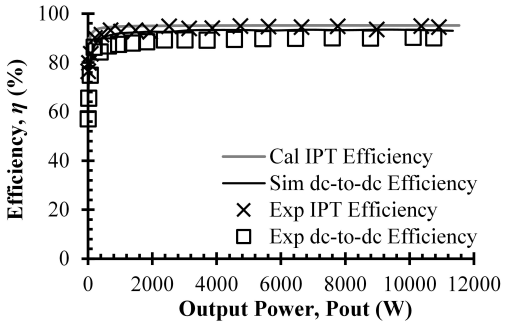

Fig. 22: *Efficiency-output power characteristics of the IPT system, and efficiency at the maximum power of 90.0%.*

Table 2: *Performance of the static IPT comparison.*

Type	Power (W)	η (%)	Air Gap (mm)	Ref.
Static	1,240	75	160	[2]
Static	12	27.3	300	[5]
Static	10	N/A	160	[6]
Static	30	N/A	0–600	[7]
Static	250 k[a]	N/A	N/A	[20]
Static	14	80	100	[41]
Static	230	N/A	70	[42]
Static	324	73.6	40	[43]
Static	82	N/A	300	[44]
Static	110	N/A	150	[45]
Static	289	80–90	120	[46]
Static	1,000	90	150–250	[47]
Static	540	N/A	0	[48]
Static	200	64	70	[49]
Static	10,750[b]	90.0	160	This Work

[a]Highest power generated by the static IPT

[b]Highest power generated by the Thai static IPT

Fig. 22 shows the similarity between the simulation and experimental results for dc-to-dc efficiency versus DC output power characteristics of the prototype 10 kW IPT system. The dc-to-dc efficiency of the prototype 10 kW system reached 90%, along with the output power of 1 kW to 10 kW. At 369.4 V DC input voltage, 32.33 A DC input current, the dc output voltage and current were 362.4 V and 29.67 A, respectively. The maximum DC output power was 10.75 kW, resulting in 90.0% dc-to-dc efficiency.

The simulated results for the IPT system DC output power and coil-to-coil efficiency using the MATLAB Simulink were slightly higher than the experimental results due to the switching losses, which were not considered in the first stage simulation model.

Table 2 shows a comparison of the output power, efficiency, and air gap between the IPT developed by Thailand and the world leaders in static IPT research. In this study, the DC output power was 10.75 kW; lower than that generated by hi-end labs in leading countries of 22 kW to 250 kW [12–20]. Therefore, Thai researchers should continue to develop the IPT to create a higher sustainable IPT level.

In previous research conducted on Thailand, [2–7, 12–20], the static IPT installed in EV charging station was no higher than 1,240 W. This is the first time that IPT development in Thailand has reached the level of 10 kW, the highest power generated for an EV charging station prototype in the country.

This work demonstrates 90.0% efficiency, matching that of the IPTs produced by hi-end labs [8–23] or previous studies on Thai IPTs [2–7, 41–49].

The next stage of development should focus on EV charging processes, and the effects of changes in the $M(x, y, z)$ when the positioning of Tx and Rx alters from the original 0, 0, 160 mm. Automatic EV charging and control could take an experimental approach.

In the future, the IPT cores should be developed using the optimization technique to achieve the highest power and efficiency at the lowest cost. Magnetic materials such as amorphous microcrystalline cores may be used at higher operating frequencies.

5. CONCLUSION

The EV market is rising despite the COVID-19 pandemic in Thailand and worldwide. The Energy Policy and Planning Office (EPPO) is promoting the EV market and supporting commercial size wireless power transfer development in Thailand. None of the proposed IPTs are currently higher than 1.24 kW in Thailand since there is an insufficient number of 3.5 kW or higher commercial chargers. This study aims to develop a 10 kW IPT for EV charging in Thailand. The block UU-shaped EE55 ferrite core design for use as a prototype 10 kW IPT has been scaled up from the previous work and not proposed by other researchers. The spiral winding of the homemade Litz wire has been designed, simulated, and measured in this study. The experimental procedure began with the Tx and Rx of the IPT prototype being simulated and measured for the M and k. Secondly, the HF frequency inverter was constructed and tested. Finally, the prototype of 10 kW IPT was constructed and characterized. The results reveal that the maximum DC power output and the dc-to-dc efficiency of the prototype IPT were 10.75 kW and 90.0%, respectively.

The advantages of the proposed method are as follows: (a) it can produce high power IPT coils, (b) it shortens the sinter casting process by using commercial EE55 ferrite cores, (c) the prototype IPT core is faster than the sintering casting ferrite core made-to-order method, (d) the prototype IPT is cost-effective since it uses the commercial ferrite core rather than the made-to-order ferrite core, (e) the ferrite core exhibits high stability in performance during installation on the EV steel chassis and structure, (f) the IPT contributes to existing knowledge on the IPT system development and experience, (g) it helps to create decision-making confidence in EV customers, and (h) the prototype proposed in this work can be used to inspire other researchers starting to study the high power IPT system.

ACKNOWLEDGMENTS

This work was supported by the Development of Wireless Electric Vehicle Battery Charging Station Project, Energy Conservation and Promotion Fund, Energy Policy and Planning Office (EPPO), Ministry of Energy, Thailand, contract of ENCONFUND 07-02-61-001/13. The authors are extremely grateful for the support of the Energy Policy and Planning Office, Ministry of Energy, Thailand. We would also like to thank the Rajamangala University of Technology Lanna (RMUTL) Chiang Mai and RMUTL Chiang Rai for their support.

REFERENCES

[1] "Global EV outlook 2021," International Energy Agency, Tech. Rep., Apr. 2021.

[2] T. Somsak, A. Namin, W. Tammawam, J. Thongpron, W. Tippachon, and K. Oranpiroj, "A prototype of block UU shape ferrite cores inductive wireless power transfer for EV charger," in *2021 18th International Conference on Electrical Engineering/Electronics, Computer, Telecommunications and Information Technology (ECTI-CON)*, 2021, pp. 930–935.

[3] T. Somsak, A. Namin, T. Sriprom, J. Thongpron, U. Kamnarn, and N. Patcharaprakiti, "Constant current - voltage with maximum efficiency inductive wireless EV charging control using dual - sides DC converters," in *2021 18th International Conference on Electrical Engineering/Electronics, Computer, Telecommunications and Information Technology (ECTI-CON)*, 2021, pp. 936–941.

[4] IEEEXplore. [Online]. Available: https://ieeexplore.ieee.org/search/searchresult.jsp?newsearch=true&queryText=wirelesspowertransfer

[5] A. Namin, E. Chaidee, T. Sriprom, and P. Bencha, "Performance of inductive wireless power transfer between using pure sine wave and square wave inverters," in *2018 IEEE Transportation Electrification Conference and Expo, Asia-Pacific (ITEC Asia-Pacific)*, 2018.

[6] A. Namin, E. Chaidee, T. Prachuabroek, T. Jumpoo, and N. Thamapanya, "Solar tricycle with lateral misalignment maximum power point tracking wireless power transfer," in *2018 15th International Conference on Electrical Engineering/Electronics, Computer, Telecommunications and Information Technology (ECTI-CON)*, 2018, pp. 656–659.

[7] A. Namin, E. Chaidee, S. Tanang, K. Chaikam, and P. Jansuya, "Mutual impedance adaptation for maximum power point tracking on LED TV wireless power transfer vary with distance," in *2018 15th International Conference on Electrical Engineering/Electronics, Computer, Telecommunications and Information Technology (ECTI-CON)*, 2018, pp. 501–504.

[8] Y. J. Jang, "Survey of the operation and system study on wireless charging electric vehicle systems,"

Transportation Research Part C: Emerging Technologies, vol. 95, pp. 844–866, Oct. 2018.

[9] A. A. Mohamed, A. A. Shaier, H. Metwally, and S. I. Selem, "A comprehensive overview of inductive pad in electric vehicles stationary charging," *Applied Energy*, vol. 262, Mar. 2020, Art. no. 114584.

[10] D. Patil, M. K. McDonough, J. M. Miller, B. Fahimi, and P. T. Balsara, "Wireless power transfer for vehicular applications: Overview and challenges," *IEEE Transactions on Transportation Electrification*, vol. 4, no. 1, pp. 3–37, Mar. 2018.

[11] H. Feng, R. Tavakoli, O. C. Onar, and Z. Pantic, "Advances in high-power wireless charging systems: Overview and design considerations," *IEEE Transactions on Transportation Electrification*, vol. 6, no. 3, pp. 886–919, Sep. 2020.

[12] WiTricity, "WiT-3300 Development Kit." Accessed Sep. 29, 2021. [Online]. Available: https://www.terraelectronica.ru/pdf/show?pdf_file=%2Fpdf%2FWITRCITY%2FWiT-3300DS.pdf

[13] "7 kW Wireless Power Transmission Technology for EV Charging." Toshiba. https://www.global.toshiba/ww/technology/corporate/rdc/rd/fields/14-e01.html (accessed Sep. 26, 2021).

[14] P. Schumann, T. Diekhans, O. Blum, U. Brenner, and A. Henkel, "Compact 7 kW inductive charging system with circular coil design," in *2015 5th International Electric Drives Production Conference (EDPC)*, 2015.

[15] WiTricity. https://witricity.com/products/automotive/ (accessed Sep. 26, 2021).

[16] J. Tritschler, S. Reichert, and B. Goeldi, "A practical investigation of a high power, bidirectional charging system for electric vehicles," in *2014 16th European Conference on Power Electronics and Applications*, 2014.

[17] J. Pries, V. P. N. Galigekere, O. C. Onar, and G.-J. Su, "A 50-kW three-phase wireless power transfer system using bipolar windings and series resonant networks for rotating magnetic fields," *IEEE Transactions on Power Electronics*, vol. 35, no. 5, pp. 4500–4517, May 2020.

[18] "ORNL demonstrates 120-kilowatt wireless charging for vehicles." Oak Ridge National Laboratory. https://www.ornl.gov/news/ornl-demonstrates-120-kilowatt-wireless-charging-vehicles (accessed Sep. 26, 2021).

[19] "Bombardier's PRIMOVE Technology Enters Service on Scandinavia's First Inductively Charged Bus Line." Bombardier. https://bombardier.com/en/media/news/bombardiers-primove-technology-enters-service-scandinavias-first-inductively-charged-bus (accessed Sep. 26, 2021).

[20] WAVE, https://waveipt.com/ (accessed Sep. 26, 2021).

[21] A. Delgado, J. A. Oliver, J. A. Cobos, J. Rodriguez, and A. Jimenez, "Optimized design for wireless coil for electric vehicles based on the use of magnetic nano-articles," in *2019 IEEE Applied Power Electronics Conference and Exposition (APEC)*, 2019, pp. 1515–1520.

[22] X. Sun, Y. Zheng, Z. Li, X. Li, and H. Zhang, "Stacked flexible parylene-based 3d inductors with ni80fe20 core for wireless power transmission system," in *2013 IEEE 26th International Conference on Micro Electro Mechanical Systems (MEMS)*, 2013, pp. 849–852.

[23] C. Carretero, I. Lope, and J. Acero, "Magnetizable concrete flux concentrators for wireless inductive power transfer applications," *IEEE Journal of Emerging and Selected Topics in Power Electronics*, vol. 8, no. 3, pp. 2696–2706, Sep. 2020.

[24] S. A. Moosavi, S. S. Mortazavi, A. Namadmalan, A. Iqbal, and M. Al-Hitmi, "Design and sensitivity analysis of dynamic wireless chargers for efficient energy transfer," *IEEE Access*, vol. 9, pp. 16 286–16 295, 2021.

[25] A. Ramezani and M. Narimani, "Optimal design of fully integrated magnetic structure for wireless charging of electric vehicles," *IEEE Transactions on Transportation Electrification*, vol. 7, no. 4, pp. 2114–2127, Dec. 2021.

[26] B. Zhang, Q. Chen, L. Zhang, J. Chen, L. Xu, X. Ren, and Z. Zhang, "Triple-coil-structure-based coil positioning system for wireless EV charger," *IEEE Transactions on Power Electronics*, vol. 36, no. 12, pp. 13 515–13 525, Dec. 2021.

[27] J. Deng, Q. Mao, W. Wang, L. Li, Z. Wang, S. Wang, and G. Guidi, "Frequency and parameter combined tuning method of LCC–LCC compensated resonant converter with wide coupling variation for EV wireless charger," *IEEE Journal of Emerging and Selected Topics in Power Electronics*, vol. 10, no. 1, pp. 956–968, Feb. 2022.

[28] K. Song, G. Yang, H. Zhang, X. Huang, J. Jiang, Y. Lan, X. Huang, J. Li, and C. Zhu, "An impedance decoupling-based tuning scheme for wireless power transfer system under dual-side capacitance drift," *IEEE Transactions on Power Electronics*, vol. 36, no. 7, pp. 7526–7536, Jul. 2021.

[29] E. Asa, O. C. Onar, V. P. Galigekere, Rong, Zeng, G.-J. Su, and B. Ozpineci, "A novel three phase oak ridge DC / AC converter for wireless grid tied applications," in *2021 IEEE Transportation Electrification Conference & Expo (ITEC)*, 2021.

[30] Y. Liu, C. Liu, X. Gao, and Y. Xiao, "Novel output regulation method for three-phase three-level wireless EV charging system," *IEEE Transactions on Magnetics*, vol. 58, no. 2, pp. 1–7, Feb. 2022.

[31] F. Sadeque and F. Fateh, "Voltage control by transmitter-side measurements for on-board wireless EV battery charger," in *2021 IEEE Kansas Power and Energy Conference (KPEC)*, 2021.

[32] W. Pairindra, P. Khemmook, and S. Khomfoi, "The implementation of fundamental harmonic ap-

proximation technique on electric vehicle wireless charger," in *2021 18th International Conference on Electrical Engineering/Electronics, Computer, Telecommunications and Information Technology (ECTI-CON)*, 2021, pp. 547–550.

[33] M. Elshaer, C. Bell, A. Hamid, and J. Wang, "DC–DC topology for interfacing a wireless power transfer system to an on-board conductive charger for plug-in electric vehicles," *IEEE Transactions on Industry Applications*, vol. 57, no. 6, pp. 5552–5561, Nov. 2021.

[34] Y. Jiang, L. Wang, J. Fang, R. Li, R. Han, and Y. Wang, "A high-efficiency ZVS wireless power transfer system for electric vehicle charging WithVariable angle phase shift control," *IEEE Journal of Emerging and Selected Topics in Power Electronics*, vol. 9, no. 2, pp. 2356–2372, Apr. 2021.

[35] A. A. S. Mohamed, D. Day, A. Meintz, and J. Myungsoo, "Real-time implementation of smart wireless charging of on-demand shuttle service for demand charge mitigation," *IEEE Transactions on Vehicular Technology*, vol. 70, no. 1, pp. 59–68, Jan. 2021.

[36] B. Zhang, J. Deng, L. Li, Z. Wang, S. Wang, and G. Guidi, "Thermal analysis and design of a 30kW EV wireless charger with liquid-cooled shell for magnetic coupler and integrated power converter," in *2021 IEEE Applied Power Electronics Conference and Exposition (APEC)*, 2021, pp. 426–431.

[37] J. C. Lin, "Safety of wireless power transfer," *IEEE Access*, vol. 9, pp. 125 342–125 347, 2021.

[38] "Get to know Thai consumers." (in Thai) Thansettakij Multimedia. https://www.thansettakij.com/content/motor/463406 (accessed May 6, 2021).

[39] Yossapong Laoonual *et al.*, "Assessment of Electric Vehicle Technology Development and Its Implication in Thailand," (in Thai) National Science and Technology Development Agency, Thailand, October 2015. [Online]. Available: http://waa.inter.nstda.or.th/stks/pub/2015/20151222-electric-vehicle.pdf

[40] "Number of EV and Charging Stations in Thailand," Electric Vehicle Association of Thailand, 2020.

[41] W. Khan-ngern and H. Zenkner, "Wireless power charging on electric vehicles," in *2014 International Electrical Engineering Congress (iEECON)*, 2014.

[42] P. Nalinnopphakhun, W. Onreabroy, and A. Kaewpradap, "Parameter effects on induction coil transmitter of wireless charging system for small electric motorcycle," in *2018 IEEE International WIE Conference on Electrical and Computer Engineering (WIECON-ECE)*, 2018, pp. 145–148.

[43] P. Jeebklum, K. Aodsup, and C. Sumpavakup, "Development of a static wireless power transfer system for electric bikes," in *2019 Research, Invention, and Innovation Congress (RI2C)*, 2019.

[44] E. Chaidee, A. Sangswang, S. Naetiladdanon, and E. Mujjalinvimut, "Influence of distance and frequency variations on wireless power transfer," in *2017 14th International Conference on Electrical Engineering/Electronics, Computer, Telecommunications and Information Technology (ECTI-CON)*, 2017, pp. 572–575.

[45] N. Hatchavanich, M. Konghirun, and A. Saengswang, "LCL — LCCL voltage source inverter with phase shift control for wireless EV charger," in *2017 IEEE 12th International Conference on Power Electronics and Drive Systems (PEDS)*, 2017, pp. 297–301.

[46] N. Hatchavanich, A. Sangswang, and M. Konghirun, "Effects of intermediate coil position in a triple-coil series-series compensation in wireless power transfer," in *2019 IEEE International Symposium on Circuits and Systems (ISCAS)*, 2019.

[47] P. Vienglek, S. Nutwong, A. Sangswang, S. Naetiladdanon, and E. Mujjalinvimut, "Comparative study of magnetically coupled coil used in dynamic wireless battery charger for electric vehicles," in *2020 23rd International Conference on Electrical Machines and Systems (ICEMS)*, 2020, pp. 1775–1778.

[48] S. Nutwong, A. Sangswang, S. Naetiladdanon, and E. Mujjalinvimut, "A novel output power control of wireless powering kitchen appliance system with free-positioning feature," *Energies*, vol. 11, no. 7, 2018, Art. no. 1671.

[49] W. Amasiri, P. Pothong, T. Pinyathanabat, and W. Pijitrojana, "Automatic efficiency maintaining system for wireless power transfer using automatic resonance frequency tuning," (in Thai) *Thai Science and Technology Journal*, vol. 25, no. 5, pp. 870–879, 2017.

[50] *Electric Vehicle Wireless Power Transfer (WPT) System – Part 1: General Requirements*, IEC 61980-1:2015, International Electrotechnical Commission, Geneva, Switzerland, July 24, 2015.

[51] Ranlo coil. https://ranlocoil.en.ecplaza.net/products (accessed Sep. 29, 2021).

[52] KAIST, "KAIST OLEV." Accessed Sep. 29, 2021. [Online]. Available: https://olev.kaist.ac.kr/_userfiles//BOARD_NOTICE/14320908091.pdf

Jutturit Thongpron received his B.S.Tech.Ed. in Electrical Engineering in 1990 from Rajamangala Institute of Technology, Chiang Mai Campus, and M.S.Tech.Ed. in Electrical Engineering from King Mongkut's Institute of Technology North Bangkok in 1994. He received his Ph.D. in Energy Technology from King Mongkut's University of Technology Thonburi, Bangkok, in 2005. He is working as Asst. Prof. of Rajamangala University of Technology Lanna, Chiang Mai. His research activity involves PV characterization, PV system, smart grid, wireless EV charging, clean energy system, and community applications technology.

Wuttikai Tammawan received his B.Eng. in Electrical Engineering in 2019 from Rajamangala University of Technology Lanna, Chiang Rai. He is working as Asst. Lecturer of Rajamangala University of Technology Lanna, Chiang Rai. His research activity involves inductive and capacitive wireless power transfer, wireless EV charging, and inductive coils design.

Kosol Oranpiroj received his B.S.Tech.Ed. Electrical Engineering in 1986 from King Mongkut's Institute of Technology North Bangkok, B.Eng. in Electrical Engineering from the Pathumwan Institute of Technology in 2004, M.Eng. (Electrical Engineering) from Chiang Mai University in 1995. He received his Ph.D. in Electrical Engineering from Chiang Mai University in 2011. He is working as Assoc. Prof. of the Rajamangala University of Technology Lanna, Chiang Mai. His research movement concentrates on power stability, clean energy system, smart grid, wireless EV charging, and community applications technology.

Teerasak Somsak received his Higher Dip. Tech. in Electrical Power in 1996 from Pathumwan Institute of Technology, Bangkok and M.Eng. in Energy Technology from King Mongkut's University of Technology Thonburi, Bangkok, in 2000. He received his Ph.D. in Electrical Engineering from Kanazawa University, Japan, in 2005. He is working as a Lecturer of Rajamangala University of Technology Lanna, Chiang Mai. His research area focuses on PV pumping, PV- battery system, smart grid, wireless EV charging, clean energy system, and community applications technology.

Ekkachai Chaidee received the B.S.Ind.Ed. (Electrical engineering) from the King Mongkut's University of Technology Thonburi (KMUTT), Bangkok, Thailand, in 2001 and the M.Sc. Eng. (Electrical engineering) from the King Mongkut's University of Technology North Bangkok (KMUTNB), Bangkok, Thailand, in 2008. He is currently pursuing the D.Eng. (Electrical and information engineering technology) with the King Mongkut's University of Technology Thonburi (KMUTT), respectively. He is working as Asst. Prof. of Rajamangala University of Technology Lanna, Chiang Rai. His current research interest includes the resonant inverter and control technique for inductive power transfer (IPT).

Wiwat Tippachon received his B.Eng. in Electrical Engineering in 1997 from King Mongkut's Institute of Technology Ladkrabang. He received his M.Eng and D.Eng in Electrical Engineering from Kasetsart University, Bangkok, in 2002 and 2009 respectively. He is working as Asst. Prof. of Rajamangala University of Technology Lanna, Chiang Rai. His research study spotlights on electric drives, optimization in electrical engineering, and wireless EV charging.

Anon Namin received the B.Sc.Ind.Ed. in Electrical Engineering from King Mongkut's Intitute of Technology Thonburi, Bangkok, Thailand, in 1996. He received and M.Sc.Ind.Ed. in Electrical Engineering and Ph.D. in Energy Technology from King Mongkut's Institute of Technology Thonburi (KMUTT), Thailand, in 2002 and 2013 respectively. He is working as Asst. Prof. in Rajamangala University of Technology Lanna (RMUTL), Chiang Rai, Thailand. His main research interests include the field of power electronic circuits and control, inductive wireless power transfer, wireless EV charging, solar simulator, photovoltaic characterization.